12-14-2011

Relating Dynamic Protein Interactions Of Metallochaperones With Metal Transfer At The Single-Molecule Level

J. J. Benítez

A. M. Keller

D. L. Huffman

Liliya A. Yatsunyk
Swarthmore College, lyatsun1@swarthmore.edu

A. C. Rosenzweig

See next page for additional authors

Relating dynamic protein interactions of metallochaperones with metal transfer at the single-molecule level

Jaime J. Benítez,[a] Aaron M. Keller,[a] David L. Huffman,[b] Liliya A. Yatsunyk,†[c] Amy C. Rosenzweig[c] and Peng Chen*[a]

Received 7th April 2010, Accepted 14th April 2010
DOI: 10.1039/c004913a

Metallochaperones undertake specific interactions with their target proteins to deliver metal ions inside cells. Understanding how these protein interactions are coupled with the underlying metal transfer process is important, but challenging because they are weak and dynamic. Here we use a nanovesicle trapping scheme to enable single-molecule FRET measurements of the weak, dynamic interactions between the copper chaperone Hah1 and the fourth metal binding domain (MBD4) of WDP. By monitoring the behaviors of single interacting pairs, we visualize their interactions in real time in both the absence and the presence of various equivalents of Cu^{1+}. Regardless of the proteins' metallation state, we observe multiple, interconverting interaction complexes between Hah1 and MBD4. Within our experimental limit, the overall interaction geometries of these complexes appear invariable, but their stabilities are dependent on the proteins' metallation state. In apo–holo Hah1–MBD4 interactions, the complexes are stabilized relative to that observed in the apo–apo interactions. This stabilization is indiscernible when Hah1′s Cu^{1+}-binding is eliminated or when both proteins have Cu^{1+} loaded. The nature of this Cu^{1+}-induced complex stabilization and of the interaction complexes are discussed. These Cu^{1+}-induced effects on the Hah1–MBD4 interactions provide a step toward understanding how the dynamic protein interactions of copper chaperones are coupled with their metal transfer function.

1. Introduction

Metals are essential for life processes, such as oxygen transport, electron transport, and hormone production.[1] They can also be toxic, however, especially at high concentrations. To maintain normal metabolism, a variety of protein machineries control the concentrations and availability of metal ions inside cells.[2–4] One type of such protein machineries mediate intracellular metal trafficking, so the metal ions can reach their functional locations while avoiding adventitious binding by many other possible molecules inside cells.[2,4–8] Intracellular copper trafficking is mediated by copper chaperones; they bind and deliver copper to their target proteins

[a]*Department of Chemistry and Chemical Biology, Cornell University, Ithaca, New York, 14853, USA. E-mail: pc252@cornell.edu*
[b]*Department of Chemistry, Western Michigan University, Kalamazoo, Michigan, 49008, USA*
[c]*Departments of Biochemistry, Molecular Biology and Cell Biology, and of Chemistry, Northwestern University, Evanston, Illinois, 60208, USA*

† Current address: Department of Chemistry and Biochemistry, Swarthmore College, 500 College Ave, Swarthmore, Pennsylvania 19081, USA

through specific and dynamic protein–protein interactions.[5,6,8–10] In human cells, the copper chaperone Hah1 (also called Atox1) delivers Cu^{1+} to the Menkes disease protein (MNK, also called ATP7A) or the Wilson disease protein (WDP, also called ATP7B), for subsequent incorporation into copper-requiring enzymes or for efflux under copper stress.[11–14]

Hah1 is a small single-domain cytoplasmic protein;[6] WDP and MNK are large, multidomain proteins anchored on organelle membranes.[13,15–18] The cytosolic N-termini of WDP and MNK both have six metal-binding domains (MBDs). All these MBDs, as well as Hah1, share the same $\beta\alpha\beta\beta\alpha\beta$ protein fold and all have the surface exposed, conserved CXXC motif, where the two cysteines bind Cu^{1+}. Upon Hah1–MBD interaction, Cu^{1+} can be transferred *via* a thiol ligand exchange mechanism at the protein interaction interface.[5,9,13,19–21]

Past studies have shown that the N-terminal MBDs of WDP and MNK have different functional roles,[13,22–32] even though all these MBDs, as well as Hah1, have similar Cu^{1+} binding affinities.[17,27,33–35] This similarity indicates that the Cu^{1+} transfer between them is under *kinetic* control mediated by protein interactions and that the functional differences among WDP (or MNK) MBDs are not defined by their Cu^{1+} binding affinity but may be related to *how* each MBD interacts with Hah1. Quantifying how Hah1 and WDP/MNK MBDs interact is thus crucial for understanding their interaction mediated copper transfer process.

Yet few quantitative measurements are available, especially on the dynamics of protein interactions of copper chaperones.[36] This scarcity comes mainly from the difficulty in conventional ensemble measurements of weak protein interactions. These weak interactions are dynamic and stochastic, making synchronization of molecular actions necessary. Often the steady-state concentrations of interaction intermediates are low, making detection difficult. Furthermore, multiple interaction intermediates, if present, convolute the ensemble-averaged measurements.

Our group has used single-molecule fluorescence resonance energy transfer (smFRET) to study the dynamic interactions of copper chaperones (Fig. 1A).[36–39] At the single-molecule level, no synchronization of molecular actions is necessary; molecular actions are followed in real time, including the formation and dissociation of interaction intermediates; and at any time point, only one molecular state is observed. We have initially focused on the interactions between Hah1 and a single MBD of WDP (the fourth MBD, MBD4). We label the two interacting proteins with a FRET donor–acceptor pair and excite the donor directly with a laser while monitoring the fluorescence intensities of both the donor (I_D) and the acceptor (I_A) simultaneously. The donor-to-acceptor FRET efficiency can be determined ($E_{FRET} \approx I_A/(I_A + I_D)$), which is directly correlated with the donor–acceptor interdistance, r, as $E_{FRET} = 1/[1 + (r/r_0)^6]$, where r_0 is the Förster radius of the donor–acceptor pair. Changes in E_{FRET} thus directly reflect the changes in the donor–acceptor interdistances and thus the protein interactions that cause these interdistance changes.

There are still technical challenges to overcome before smFRET can be applied to follow *weak* protein interactions *in real time*. The primary challenge is the concentration limit: single-molecule measurements are typically performed at pM–nM concentrations of fluorescently labeled species to separate them spatially. Weak protein interactions, including those of copper chaperones with $K_D \sim \mu M$, need to be studied at much higher concentrations ($> \mu M$) to favor complex formation. Moreover, to follow the same protein molecules interacting in real time, they need to be surface immobilized, where their nonspecific interactions with surfaces must be minimized.

We have used a nanovesicle trapping scheme[40–42] to overcome the above two challenges (Fig. 1A).[37–39] Because of the confined volume ($\sim 10^{-19}$ L) of a nanovesicle, each molecule of an interacting pair inside has an effective concentration of a few μM (see Experimental Section). The overall number of nanovesicles is kept low to separate them spatially to ensure single-nanovesicle (*i.e.*, single-pair) detection.

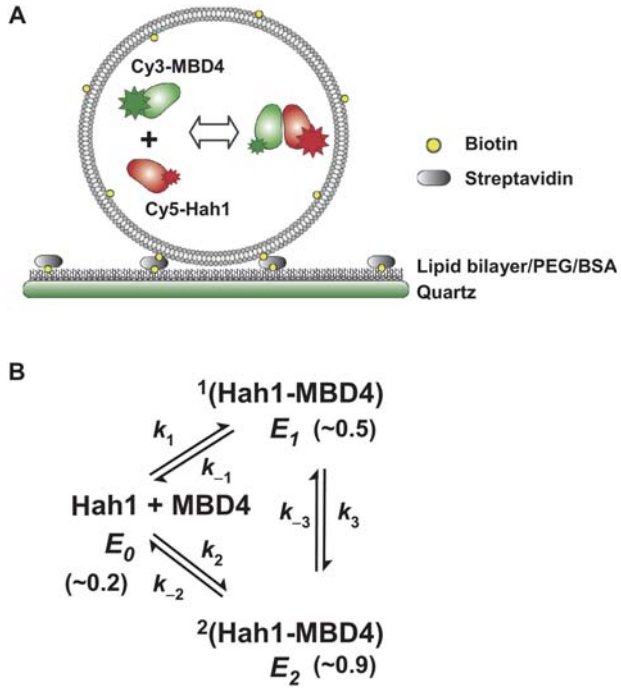

Fig. 1 (A) Schematic of nanovesicle trapping of Cy5-Hah1 and Cy3-MBD4 for smFRET studies. The inner diameter of the nanovesicle is 80 ± 20 nm. The glass surface is coated with biotinylated lipid bilayer, PEG, or BSA to prevent vesicle rupture. (B) Interaction scheme between apo-forms of Hah1 and MBD4. Besides the dissociated state, there are two interaction complexes that interconvert dynamically. k's are rate constants. k_1 and k_2: $\sim 10^5$ M^{-1} s^{-1}; k_{-1}, k_{-2}, k_3, and k_{-3}: $\sim 10^0$ s^{-1}.[37,38]

The nanovesicles are then immobilized on the surface, where possible nonspecific interactions of the proteins with the glass surface are eliminated. Although we cannot ensure that every nanovesicle will contain two different protein molecules, we can control the statistical distribution of molecules in nanovesicles, and for each nanovesicle, the number and type of molecules inside can be determined from their photobleaching events.[37,39] By examining only the nanovesicles containing two different molecules, we can eliminate interactions between molecules of the same type, which is not possible in ensemble experiments and significantly complicates protein interaction studies. This complication is particularly relevant for copper chaperones, as they can form dimers in solution.[43]

Using the nanovesicle trapping scheme combined with smFRET measurements, we have observed real-time interaction events between a single pair of Hah1 and WDP MBD4.[37,38,39] More important, we have identified that even in the absence of Cu^{1+}, Hah1 and MBD4 can form two interaction complexes, which interconvert dynamically (Fig. 1B). One complex has an E_{FRET} value of ~0.5 (E_1), the other of ~0.9 (E_2), besides their dissociated state (E_0 ~0.2). The significant difference in the E_{FRET} values of these two complexes further suggests that they likely have different overall interaction geometries. The results have also enabled us to quantify the kinetics of association, dissociation, and interconversion of the two interaction complexes, as well as their dissociation constants.

The existence of multiple interaction complexes between Hah1 and a WDP MBD has functional implications. Inside cells, copper chaperones encounter their target proteins through diffusion. The initial encounter pair often rapidly returns to the dissociated form. The ability to form multiple interaction complexes with different

geometries increases the probability of complex formation. The formed complex, if productive, may proceed to accomplish Cu^{1+} transfer, or, if unproductive, can convert to the other complex for Cu^{1+} transfer. The interconversion kinetics of Hah1–MBD4 complexes are comparable to their dissociation kinetics (k_3 and k_{-3} *versus* k_{-1} and k_{-2}, Fig. 1B), further supporting this possible mechanism of operation.

Still, many questions remain. For example, how are the Hah1–MBD interactions coupled with the Cu^{1+} transfer process? Of the two interaction complexes, which one is productive for metal transfer, or are both so? Do Hah1 and a WDP MBD still form multiple complexes in the presence of Cu^{1+}? To address these questions, observing Cu^{1+} transfer directly during protein interaction would be ideal, but is challenging because the d^{10} electron configuration of Cu^{1+} makes it magnetically silent and optically invisible except for X-ray-based techniques. Our smFRET measurements cannot directly observe Cu^{1+} transfer, either. Nevertheless, as we are able to study the protein interactions in real time and quantitatively, we can examine the effects of Cu^{1+} on the interaction dynamics between Hah1 and a WDP MBD. Changes in the protein interaction dynamics should inform how the copper chaperone interactions are coupled with the underlying Cu^{1+} transfer process. Here we report our initial results along this line. We show how Cu^{1+} affects the formation and stability of Hah1–MBD4 interaction complexes and how the effects are related to the Cu^{1+} binding ability of Hah1.

2. Experimental section

Protein expression, purification, labeling, and mutation

Hah1 and WDP MBD4 were expressed, purified, and labeled as previously described.[37] Both proteins have a C-terminal cysteine introduced *via* site-directed mutagenesis for labeling with a fluorescent probe using maleimide chemistry. Hah1 is labeled with the FRET acceptor Cy5 at Cys69, and MBD4 is labeled with the FRET donor Cy3 at Cys76. The Cu^{1+}-binding cysteines in Hah1 and MBD4 are protected from labeling by coordinating to Cu^{1+} or Hg^{2+}, which can be removed afterwards using BCA or CN^- (for Cu^{1+}) and EDTA (for Hg^{2+}) as chelators.

The mutant Hah1, mHah1, has the two Cu^{1+}-binding cysteines in its CXXC motif (Cys12 and Cys15) mutated to serines to eliminate its Cu^{1+} binding. The mutation was confirmed by DNA sequencing and MALDI mass spectrometry of the purified protein product (MW: calculated, 7325.3 Da; observed, 7325.0 Da).

Protein concentrations were quantified using the BCA and Bradford assays with BSA as a standard (Pierce), and the thiol quantitation method (Molecular Probes). Copper concentrations were quantified using a BCA-based method by Brenner and Harris[44] and a copper atomic absorption standard solution (Acros Organics).

Nanovesicle trapping

Nanovesicle trapping was performed as previously described.[37,39] A mixture of L-α-phosphatidylcholine (eggPC) and 1% 1,2-dipalmitoyl *sn*-glycero3-phosphoethanolamine-*N*-(cap biotinyl) (16 : 0 biotinyl cap PE) (Avanti Lipids) in chloroform was dried under a constant flow of nitrogen. Protein-loaded vesicles were prepared by hydrating the lipid film with solutions containing 3 μM Cy5-Hah1, 3 μM Cy3-MBD4, 1 mM Trolox (Sigma), and 15–20 μM TCEP (Sigma) in 60 mM MES, 110 mM NaCl, pH 6.0 buffer, followed by seven freeze-thaw cycles to increase the encapsulation efficiency. Protein integrity after freeze-thaw cycles was confirmed by circular dichroism spectroscopy. The solution was then repeatedly extruded through a polycarbonate membrane with 100 nm pores (Avanti Mini Extruder) to form approximately 100-nm diameter unilamellar vesicles encapsulating proteins. Loaded vesicles were used for experiments immediately or within 48 h of preparation.

To prepare the copper-loaded proteins, the proteins were first incubated for 30 min with 15–20 μM TCEP to reduce the proteins, followed by 1 h incubation with appropriate equivalents of Cu^{1+} ($[Cu(CH_3CN)_4]PF_6$ (Aldrich) in 50% acetonitrile). The solution was then used to hydrate the dry lipid film and incubated for 1 h for nanovesicle encapsulation.

The size of the nanovesicles was measured to be 90 ± 20 nm by dynamic light scattering (Malvern Zetasizer Nano-ZS; the error bar here is the standard deviation). Taking into account the lipid bilayer thickness of ~5 nm,[45] the resulting nanovesicles have an inner diameter of 80 ± 20 nm. The corresponding effective concentration for a single molecule trapped inside is thus 6 ± 5 μM.

Single-molecule FRET measurements

Single-molecule FRET measurements were performed on a homebuilt prism-type total internal reflection microscope as described previously.[38] Briefly, a continuous wave circularly polarized 532 nm laser beam was used to directly excite the Cy3 probe. The fluorescence of Cy3 and Cy5 was collected, filtered to reject laser light, and split into two wavelength channels. Each channel of fluorescence was further filtered and projected onto half of the imaging area of a camera, operating at 50–200 ms frame rate. At 30 s prior to the end of data collection, the sample was illuminated with a 637 nm laser to directly excite the Cy5 fluorescence for determining its number within nanovesicles.[39] Single-molecule fluorescence intensity trajectories were extracted from the recorded movie, from which the E_{FRET} trajectories were calculated. Only the portions of the trajectories during 532 nm laser illumination and before the photobleaching events of the probes were analyzed.

A flow cell, formed by double-sided tape placed between a quartz slide and a coverslip, was used to hold aqueous sample solutions for single-molecule fluorescence measurements. All samples were in 60 mM MES, pH 6.0, 110 mM NaCl, 15–20 μM TCEP unless indicated otherwise. The TCEP was present to ensure a reducing environment to prevent air oxidation of Cu^{1+}. To form the bilayer support,[37,39] unloaded vesicles were flowed in at 5 mg mL^{-1} (500 μL) and incubated for 1 to 2 h. Excess lipids were washed away with standard lipid buffer. Alternatively, the slides were first amine-functionalized (Vectabond, Vector Laboratories) and then coated with PEG polymers (100 mg mL^{-1} m-PEG-SPA-5000 and 1 mg mL^{-1} biotin-PEG-NHS-3400, Nektar Therapeutics).[39,46] 1% of the PEG polymers contain a biotin terminal group to form biotin-streptavidin (Molecular Probes) linkages. We also used biotinylated BSA to coat the quartz surface:[39] a solution of 1 mg mL^{-1} biotinylated BSA was incubated on the quartz slide for 30 min to 1 h. Excess biotinylated BSA was then washed out with buffer. 500 μL of streptavidin at a concentration of 0.2 mg mL^{-1} was then flowed in and incubated for 10 min. Unbound streptavidin was then washed out with buffer containing 0.1 mg mL^{-1} BSA, which help to block nonspecific binding sites.[47] Protein-loaded vesicles were flowed in at a total protein concentration of 30 pM and unbound vesicles were then washed out before single-molecule imaging experiments. An oxygen scavenging system (0.1 mg mL^{-1} glucose oxidase (Sigma), 0.025 mg mL^{-1} catalase (Roche), 4% glucose (Aldrich) and 1 mM Trolox (Sigma)[48] was added into the sample solution just before each experiment to prolong the lifetime of the fluorescence probes, and was refreshed during experiments every half an hour.

3. Results and analysis

Observation of Hah1–MBD4 interactions in the presence of Cu^{1+} and identification of interaction complexes

We applied nanovesicle trapping in combination with smFRET to study Hah1–MBD4 interactions in the presence of Cu^{1+}. We first added one equivalent of Cu^{1+} per Hah1–MBD4 pair in preparing nanovesicle trapped molecules. As Hah1 and

MBD4 have similar Cu^{1+} binding affinities and their Cu^{1+} transfer is reversible,[23,27] approximately half of the molecules of each protein have a Cu^{1+} bound at their CXXC sites at this condition. Therefore, among a population of Hah1–MBD4 pairs trapped inside vesicles, there are pairs of apo–apo, apo–holo (*i.e.*, either Hah1 or MBD4 has a Cu^{1+} bound), and holo–holo proteins; and for a particular Hah1–MBD4 pair, it can be in either one of these three Cu^{1+}-loading states.

Fig. 2A shows an exemplary E_{FRET} trajectory of a single Hah1–MBD4 pair inside a nanovesicle in the presence of one equivalent of Cu^{1+}. The temporal E_{FRET} fluctuations report the dynamic interactions between Hah1 and MBD4. Three distinct E_{FRET} states are observed in this trajectory at E_{FRET} ~0.2, ~0.5, and ~0.8, similar to the dissociated state (E_0 ~0.2) and the two interaction complexes (E_1 ~0.5 and E_2 ~0.8) observed for Hah1–MBD4 interactions in the absence of Cu^{1+}.[37,38]

Owing to the finite trajectory length (up to 1–2 min) limited by the photobleaching of the fluorescent probes, many E_{FRET} trajectories only show two E_{FRET} states within their time span. For the same reason, it is difficult to determine reliably the E_{FRET} values of all three states from a *single* E_{FRET} trajectory. To distinguish these three states and determine their E_{FRET} values with statistical reliability, we used a 2-dimensional histogram analysis of E_{FRET} values. For each of the E_{FRET} trajectories that show merely two states, we calculated the average E_{FRET} value of each state and assigned the smaller value as E_{low} and the larger value as E_{high}. We then plotted the 2-dimensional histogram of these two E_{FRET} values from many trajectories (Fig. 3B). For those E_{FRET} trajectories that have three states and thus three E_{FRET} values, we used any two out of the three values (there are three possible combinations of selecting two values out of three), assigned them as E_{low} and E_{high} based on their relative magnitudes, and added them onto the 2-dimensional histogram. Combining results from hundreds of single Hah1–MBD4 pairs, the resulting 2-dimensional histogram shows three distinct populations (Fig. 3B), definitively indicating the presence of three E_{FRET} states in Hah1–MBD4 interactions in the presence of one equivalent of Cu^{1+}. These three populations are centered at the positions of (E_0, E_1), (E_0, E_2), and (E_1, E_2) in the 2-dimensional histogram (Fig. 3B). Projecting this 2-dimensional histogram onto the x,y axes and Gaussian-fitting the projections give the reliable E_{FRET} values for the three states: $E_0 = 0.13 \pm 0.06$, $E_1 = 0.50 \pm 0.08$, and $E_2 = 0.8 \pm 0.1$. For reference, the 2-dimensional histogram from single-pair apo–Hah1 ↔ apo–MBD4 interactions is shown in Fig. 3A, from

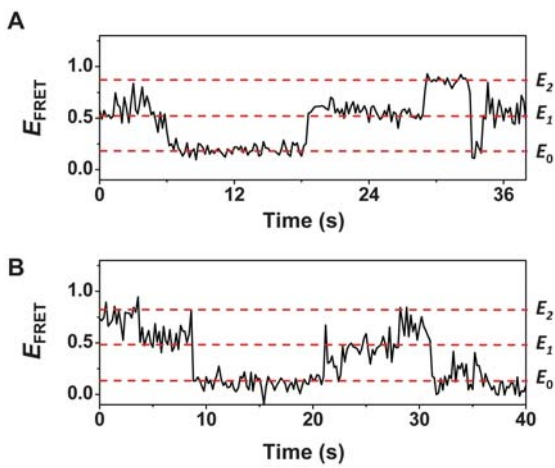

Fig. 2 Exemplary E_{FRET} trajectories of a Cy5-Hah1 and a Cy3-MBD4 inside a nanovesicle in the presence of one equivalent (A) and four equivalents of Cu^{1+} (B). Trajectories are at 200 ms time resolution.

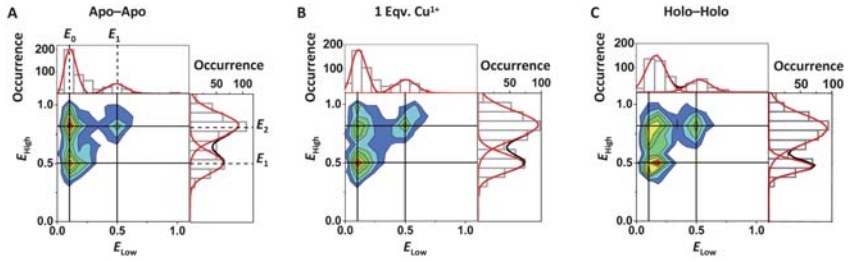

Fig. 3 2-Dimensional histograms of E_{FRET} values of Hah1 ↔ MBD4 interaction states. (A) apo–apo interactions. (B) In the presence of one equivalent of Cu^{1+}. (C) In the presence of four equivalents of Cu^{1+}. E_{low}, the E_{FRET} value of the lower FRET state; E_{high}, the E_{FRET} value of the higher FRET state in an E_{FRET} trajectory. The projections of the histograms on the x,y axes are Gaussian resolved to determine the E_{FRET} values of the three states: (A) $E_0 = 0.14 \pm 0.07$, $E_1 = 0.50 \pm 0.08$, $E_2 = 0.8 \pm 0.1$; (B) $E_0 = 0.13 \pm 0.06$, $E_1 = 0.50 \pm 0.08$, $E_2 = 0.8 \pm 0.1$; (C) $E_0 = 0.15 \pm 0.08$, $E_1 = 0.48 \pm 0.07$, $E_2 = 0.8 \pm 0.1$. Data compiled from 309 (A), 420 (B), and 249 (C) Hah1–MBD4 interacting pairs.

which the determined E_{FRET} values are $E_0 = 0.14 \pm 0.07$, $E_1 = 0.50 \pm 0.08$, and $E_2 = 0.8 \pm 0.1$, consistent with what we reported previously.[37]

At one equivalent of Cu^{1+}, there is a mixture of apo–apo, apo–holo, and holo–holo pairs of Hah1–MBD4. Consequently, the observed E_1 and E_2 states here could just be the two complexes from apo–apo interactions in the population, and it is not yet clear if apo–holo and holo–holo interactions will also form multiple complexes.

To probe pure holo–holo interactions, we added four equivalents of Cu^{1+} per Hah1–MBD4 pair. The extra equivalents of Cu^{1+} are to ensure full occupation of the proteins' copper binding sites. Further increasing the Cu^{1+} equivalents to six does not cause any significant changes in the Hah1–MBD4 interactions (such as the histogram of the E_{FRET} trajectories; see below), indicating that both proteins are already metallated in the presence of four equivalents of Cu^{1+}.

Fig. 2B shows an exemplary E_{FRET} trajectory of a single holo–holo pair. Again, three states are observed at $E_{FRET} \sim 0.2$, ~ 0.5, and ~ 0.8, corresponding to the dissociated state and the two interaction complexes, respectively. The 2-dimensional histogram of E_{FRET} values definitively shows the three-state behavior of holo–holo Hah1–MBD4 interactions (Fig. 3C). Therefore, the presence of multiple interaction complexes is general for both holo–holo and apo–apo interactions between Hah1 and MBD4. Furthermore, the E_{FRET} values of the two holo–holo interaction complexes are the same within experimental error as those of apo–apo interactions (Fig. 3C *versus* A), indicating that the overall interaction geometries of the complexes are unperturbed by Cu^{1+} binding in both proteins. Similarly, apo–holo interactions between Hah1 and MBD4 also form two complexes, as will be shown below.

Cu^{1+}-induced stabilization of apo–holo interaction complexes

The real-time E_{FRET} trajectories of single-pair Hah1–MBD4 interactions also contain information about the stabilities of their complexes. Fig. 4A–C show the histograms of the E_{FRET} trajectories of Hah1–MBD4 interactions when they are in their apo-forms, in the presence of one equivalent of Cu^{1+}, and in their holo-forms, respectively. All three histograms can be fitted by three Gaussian peaks, centered at E_0, E_1 and E_2, corresponding to the dissociated state and the two interaction complexes, respectively. As the three peaks are not clearly resolved in these histograms, the peak locations were constrained to improve the reliability of the Gaussian fits, using the E_{FRET} values determined from the analyses of the 2-dimensional E_{FRET} histograms (Fig. 3). The relative areas of the three peaks in each

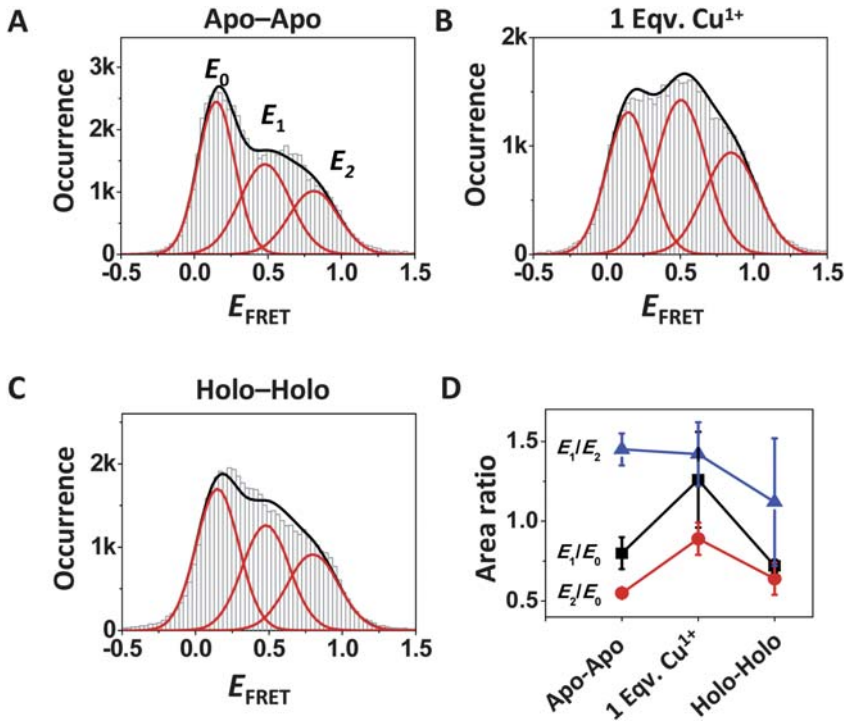

Fig. 4 (A, B, C) Histograms of E_{FRET} trajectories of single-pair Hah1–MBD4 interactions in the absence (A), or in the presence of one equivalent (B), or four equivalents of Cu^{1+} (C). Data compiled from 309 (A), 420 (B), and 249 (C) Hah1–MBD4 interacting pairs. Each histogram is fitted with three Gaussian peaks, whose centers are set to the E_{FRET} values determined from Fig. 3. (D) The area ratios of the Gaussian-resolved peaks from A, B, and C.

histogram represent the relative stabilities of the relevant states. For the apo–apo Hah1–MBD4 interactions (Fig. 4A), the calculated dissociation constants of the two complexes are $K_{D1} \sim 3 \pm 6$ μM and $K_{D2} \sim 5 \pm 9$ μM (the large error bars here mainly result from the size dispersion of the nanovesicles (inner diameter 80 ± 20 nm; see Experimental Section), from which the effective concentration of a single molecule inside is calculated).[37,38]

For holo–holo Hah1–MBD4 interactions, the relative areas of the three peaks in the histogram of E_{FRET} trajectories are similar to those of apo–apo interactions (Fig. 4C *versus* 4A, and 4D). Therefore, there is no change in stability for both the E_1 and the E_2 complex when both proteins are loaded with Cu^{1+}.

In contrast, in the presence of one equivalent of Cu^{1+}, significant changes are observed in the relative areas of the three peaks in the histogram of E_{FRET} trajectories, as compared with those of apo–apo Hah1–MBD4 interactions (Fig. 4B *versus* 4A). Both the E_1 and the E_2 peak increase in their areas relative to that of the E_0 peak, indicating an increase in the stabilities of the two interaction complexes (Fig. 4D). At one equivalent of Cu^{1+}, the Hah1–MBD4 pairs contain a mixture of apo–apo, apo–holo, and holo–holo forms. As each of the two complexes has similar stability in apo–apo and holo–holo Hah1–MBD4 interactions, the increase in the stabilities of the two complexes here must come from the contribution of apo–holo interactions. Therefore, apo–holo interactions between Hah1 and MBD4 also form two complexes, both of which are stabilized relative to those in the apo–apo interaction.

Interestingly, in the presence of one equivalent of Cu^{1+}, the E_1/E_2 peak area ratio stays essentially the same as that in the apo–apo interactions (Fig. 4D). This indicates that the two complexes are stabilized to a similar extent in apo–holo interactions, as compared with those in apo–apo interactions.

Hah1 mutation eliminates Cu^{1+}-induced stabilization of complexes

To probe if the observed Cu^{1+} stabilization effects on apo–holo Hah1–MBD4 interactions are specific to their Cu^{1+} binding and transfer, we created a Hah1 mutant, mHah1, in which the two cysteines in the CXXC motif have been mutated to serines. Therefore, mHah1 cannot bind Cu^{1+} or accept Cu^{1+} from MBD4. Fig. 5A shows the histogram of E_{FRET} trajectories of single-pair mHah1–MBD4 interactions in their apo-forms. Three E_{FRET} states are observed, corresponding to the dissociated state (E_0 ~0.2) and the two interaction complexes (E_1 ~0.5 and E_2 ~0.8). The relative areas of the three E_{FRET} peaks in the histogram are the same as those of apo–apo Hah1–MBD4 interactions, indicating that the cysteines in the CXXC motif of Hah1 are nonessential for the formation and the stability of apo–apo interaction complexes.

In the presence of one equivalent of Cu^{1+}, MBD4 can bind Cu^{1+}, whereas mHah1 cannot. Thus, no Cu^{1+} transfer between mHah1 and MBD4 can occur. The histogram of E_{FRET} trajectories of their single-pair interactions still shows three states, and no significant changes are observed in either the positions of the three peaks or their relative areas (Fig. 5B). Therefore, the Cu^{1+}-binding by Hah1 and/or processes associated with Cu^{1+}-transfer between Hah1 and MBD4 are responsible for the Cu^{1+}-induced stabilization of E_1 and E_2 complexes in the apo–holo Hah1–MBD4 interactions.

4. Discussion

Using nanovesicle trapping combined with smFRET measurements, we have examined the dynamic interactions between single pairs of Hah1 and WDP MBD4 in the absence and the presence of Cu^{1+}. The apo–apo, apo–holo, and holo–holo interactions of Hah1 and MBD4 all lead to formation of two interaction complexes that interconvert dynamically. The stabilities of the two complexes do not change when both Hah1 and MBD4 are in their holo-forms, as compared with when both are in their apo-forms (Fig. 4A, C). In contrast, when one protein is loaded with Cu^{1+}, *i.e.*, in the apo–holo interactions, stabilization of both complexes is

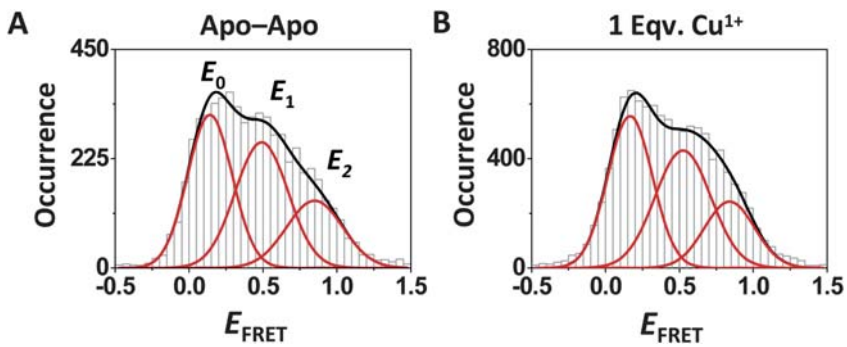

Fig. 5 Histograms of E_{FRET} trajectories of single-pair mHah1–MBD4 interactions in the absence (A) and in the presence of one equivalent of Cu^{1+} (B). Each histogram is fitted with three Gaussian peaks, whose centers are set to the E_{FRET} values determined from the 2-dimensional E_{FRET} value analyses of the smFRET trajectories as in Fig. 3.

observed (Fig. 4B). This stabilization is abolished when the Cu^{1+} binding ability (and thus the Cu^{1+} transfer ability) of Hah1 is eliminated by mutating the cysteines in its CXXC motif (Fig. 5). Interestingly, the Cu^{1+} effects on the apo–holo Hah1–MBD4 interactions do not differentiate the two interaction complexes; both the E_1 and the E_2 complex are stabilized to a similar extent (Fig. 4A, B).

Fundamentally, the Cu^{1+}-induced stabilization of protein complexes can be approximately divided into two types: one direct contribution, where the Cu^{1+} can bridge the two proteins at the interface *via* bonding with cysteines from both proteins; the other indirect contribution, where the Cu^{1+} binding to a protein causes changes in the protein's conformation, leading to better complex formation. The direct contribution is possible for apo–holo Hah1–MBD4 interactions, in which one Cu^{1+} is coordinated by cysteine ligands from both interacting partners, as described in the thiol ligand exchange mechanism for copper chaperone mediated copper transfer.[5,19,43] This metal-bridging was directly supported by the crystal structure of a Cu^{1+}-bridged Hah1 dimer[20] and the NMR structure of a Cu^{1+}-bridged complex between Hah1 and a MBD of MNK protein (Fig. 6),[49] as well as by computational studies.[50] This Cu^{1+} bridging is not applicable for holo–holo interactions, though, as both proteins here would have Cu^{1+} bound at their CXXC sites; consistently, no stabilization of protein complexes is observed in holo–holo Hah1–MBD4 interactions (Fig. 4C).

The indirect contribution is likely not to play a significant role in stabilizing either Hah1–MBD4 complex. This comes from the results on holo–holo Hah1–MBD4 interactions, where only the indirect contribution is possible, but for which no stabilization of any protein complexes is observed (Fig. 4C *versus* A).

Using the NMR structure of the Cu^{1+}-bridged Hah1–MBD complex (Fig. 6)[50] and knowing that our Cy3–Cy5 pairs are located at the C-termini, the estimated Cy3–Cy5 distance in this complex is ~5 nm. Using an E_{FRET} *versus* distance calibration curve (unpublished results), this distance corresponds to an E_{FRET} of ~0.5, similar to E_1. Therefore, the E_1 complex between Hah1 and MBD4 could be associated with the interaction geometry shown by this NMR structure. In the E_2 complex, the Hah1 and MBD4 need to interact in a way that the distance between their C-termini is closer than that in the structure in Fig. 6 to have a larger E_{FRET} value (~0.8). At the moment, we do not know the structural identity of the E_2 complex. SmFRET measurements only report structural differences along the coordinate of the donor–acceptor interdistance. Future smFRET studies, where Cy3–Cy5 are tagged at various locations on Hah1 and MBD4 to probe the structure of their complexes along multiple coordinates, may provide more information.

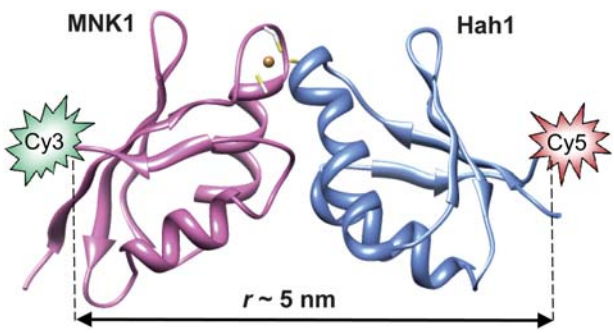

Fig. 6 NMR structure (pdb code: 2K1R)[50] of a Cu^{1+}-bridged complex between Hah1 and the first MBD of MNK. The positions corresponding to where the Cy3 and Cy5 are labeled are indicated; the anchor-to-anchor distance between the two labels is ~5 nm.

5. Conclusion

Using a nanovesicle trapping scheme in combination with smFRET measurements, we have studied the weak, dynamic interactions between the copper chaperone Hah1 and the MBD4 of WDP in the absence and the presence of various equivalents of Cu^{1+}. We have visualized their interaction events in real time and identified their interaction complexes. Regardless of their metallation state, Hah1 and MBD4 can form two complexes that interconvert dynamically, an advantageous feature for their Cu^{1+}-transfer function. Within the limit of smFRET in resolving structural differences along the coordinate of the FRET donor-to-acceptor interdistance, the interaction geometries in these two complexes appear invariable. The stabilities of the two interaction complexes are dependent on the proteins' metallation state, though. When only one of the proteins has Cu^{1+} bound (*i.e.*, apo–holo Hah1–MBD4 interactions), both complexes are stabilized relative to that observed in the apo–apo interactions. Cu^{1+}-bridging at the protein interface *via* bonding to cysteines from both proteins is likely the cause of this stabilization. Consistently, this Cu^{1+}-induced stabilization of interaction complexes is indiscernible when the Cu^{1+}-binding cysteines in Hah1 are mutated to serines to eliminate its Cu^{1+} binding ability or when both proteins have Cu^{1+} bound (*i.e.*, holo–holo Hah1–MBD4 interactions). Based on its E_{FRET} value, one of the complexes can be associated with a Hah1–MBD4 interaction complex where the CXXC motifs from the two proteins face each other to offer cysteine binding to a bridging Cu^{1+} ion. The structure of the other complex is not yet clear. These Cu^{1+}-induced effects on the Hah1–MBD4 interactions provide a step toward understanding how the dynamic protein interactions of copper chaperones are coupled with their metal transfer function.

Acknowledgements

We thank the National Institute of Health (GM082939), National Science Foundation (CHE0645392), Camille and Henry Dreyfus New Faculty Award, and Alfred F. Sloan Research Fellowship for funding our research. J. J. B. and A. M. K. were partially supported by National Institute of Health Molecular Biophysics Traineeships. We also thank Feng Gao for assistance in data analysis and Debashis Panda for sharing the results of dynamic light scattering measurements of nanovesicle size distribution.

References

1 S. J. Lippard and J. M. Berg, *Principles of Bioinorganic Chemistry*, University Science Books, Mill Valley, 1994.
2 K. J. Waldron, J. C. Rutherford, D. Ford and N. J. Robinson, *Nature*, 2009, **460**, 823–830.
3 S. C. Andrews, A. K. Robinson and F. Rodriguez-Quinones, *FEMS Microbiol. Rev.*, 2003, **27**, 215–237.
4 L. A. Finney and T. V. O'Halloran, *Science*, 2003, **300**, 931–936.
5 T. V. O'Halloran and V. C. Culotta, *J. Biol. Chem.*, 2000, **275**, 25057–25060.
6 A. C. Rosenzweig, *Acc. Chem. Res.*, 2001, **34**, 119–128.
7 P. S. Donnelly, Z. Xiao and A. G. Wedd, *Curr. Opin. Chem. Biol.*, 2007, **11**, 128–133.
8 N. J. Robinson and D. R. Winge, *Annu. Rev. Biochem.*, 2010, **79**, 537–562.
9 D. L. Huffman and T. V. O'Halloran, *Annu. Rev. Biochem.*, 2001, **70**, 677–701.
10 L. Banci and A. Rosato, *Acc. Chem. Res.*, 2003, **36**, 215–221.
11 P. C. Bull, G. R. Thomas, J. M. Rommens, J. R. Forbes and D. W. Cox, *Nat. Genet.*, 1993, **5**, 327–337.
12 I. Hamza, M. Schaefer, L. W. J. Klomp and J. D. Gitlin, *Proc. Natl. Acad. Sci. U. S. A.*, 1999, **96**, 13363–13368.
13 D. Larin, C. Mekios, K. Das, B. Ross, A.-S. Yang and T. C. Gilliam, *J. Biol. Chem.*, 1999, **274**, 28497–28504.
14 J. M. Walker, R. Tsivkovskii and S. Lutsenko, *J. Biol. Chem.*, 2002, **277**, 27953–27959.
15 L. Banci, I. Bertini, F. Cantini, C. Massagni, M. Migliardi and A. Rosato, *J. Biol. Chem.*, 2009, **284**, 9354–9360.

16 S. Lutsenko, K. Petrukhin, M. J. Cooper, T. C. Gilliam and J. H. Kaplan, *J. Biol. Chem.*, 1997, **272**, 18939–18944.
17 L. Banci, I. Bertini, F. Cantini, N. Della-Malva, M. Migliardi and A. Rosato, *J. Biol. Chem.*, 2007, **282**, 23140–23146.
18 Y. Yamaguchi, M. E. Heiny, M. Suzuki and J. D. Gitlin, *Proc. Natl. Acad. Sci. U. S. A.*, 1996, **93**, 14030–14035.
19 R. A. Pufahl, C. P. Singer, K. L. Peariso, S.-J. Lin, P. J. Schmidt, C. J. Fahrni, V. C. Culotta, J. E. Penner-Hahn and T. V. O'Halloran, *Science*, 1997, **278**, 853–856.
20 A. K. Wernimont, D. L. Huffman, A. L. Lamb, T. V. O'Halloran and A. C. Rosenzweig, *Nat. Struct. Biol.*, 2000, **7**, 766–771.
21 F. Arnesano, L. Banci, I. Bertini and M. J. J. Bonvin, *Structure*, 2004, **12**, 669–676.
22 L. Banci, I. Bertini, F. Cantini, C. T. Chasapis, N. Hadjiliadis and A. Rosato, *J. Biol. Chem.*, 2005, **280**, 38259–38263.
23 D. Achila, L. Banci, I. Bertini, J. Bunce, S. Ciofi-Baffoni and D. L. Huffman, *Proc. Natl. Acad. Sci. U. S. A.*, 2006, **103**, 5729–5734.
24 D. Huster and S. Lutsenko, *J. Biol. Chem.*, 2003, **278**, 32212–32218.
25 S. Lutsenko, E. S. LeShane and U. Shinde, *Arch. Biochem. Biophys.*, 2007, **463**, 134–148.
26 J. M. Walker, D. Huster, M. Ralle, C. T. Morgan, N. J. Blackburn and S. Lutsenko, *J. Biol. Chem.*, 2004, **279**, 15376–15384.
27 L. A. Yatsunyk and A. C. Rosenzweig, *J. Biol. Chem.*, 2007, **282**, 8622–8631.
28 E. M. W. M. van Dongen, L. W. J. Klomp and M. Merkx, *Biochem. Biophys. Res. Commun.*, 2004, **323**, 789–795.
29 I. H. Hung, R. L. B. Casareno, L. Gilles, F. S. Mathews and J. D. Gitlin, *J. Biol. Chem.*, 1998, **273**, 1749–1754.
30 D. Strausak, M. K. Howies, S. D. Firth, A. Schlicksupp, R. Pipkorn, G. Multhaup and J. F. B. Mercer, *J. Biol. Chem.*, 2003, **278**, 20821–20827.
31 D. Strausak, S. L. Fontaine, J. Hill, S. D. Firth, P. J. Lockhart and J. F. B. Mercer, *J. Biol. Chem.*, 1999, **274**, 11170–11177.
32 I. Voskoboinik, D. Strausak, M. Greenough, H. Brooks, M. Petris, S. Smith, J. F. Mercer and J. Camakaris, *J. Biol. Chem.*, 1999, **274**, 22008–22012.
33 D. L. Huffman and T. V. O'Halloran, *J. Biol. Chem.*, 2000, **275**, 18611–18614.
34 L. Banci, I. Bertini, R. Del Conte, M. D'Onofrio and A. Rosato, *Biochemistry*, 2004, **43**, 3396–3403.
35 L. Banci, I. Bertini, F. Cantini, M. Migliardi, A. Rosato and S. Wang, *J. Mol. Biol.*, 2005, **352**, 409–417.
36 P. Chen, N. M. Andoy, J. J. Benitez, A. M. Keller, D. Panda and F. Gao, *Nat. Prod. Rep.*, 2010, **27**, 757–767.
37 J. J. Benitez, A. M. Keller, P. Ochieng, L. A. Yatsunyk, D. L. Huffman, A. C. Rosenzweig and P. Chen, *J. Am. Chem. Soc.*, 2008, **130**, 2446–2447.
38 J. J. Benitez, A. M. Keller, P. Ochieng, L. A. Yatsunyk, D. L. Huffman, A. C. Rosenzweig and P. Chen, *J. Am. Chem. Soc.*, 2009, **131**, 871.
39 J. J. Benitez, A. M. Keller and P. Chen, *Meth. Enzymol.*, 2010, **472**, 41–60.
40 D. T. Chiu, C. F. Wilson, A. Karlsson, A. Danielsson, A. Lundqvist, A. Strömberg, F. Ryttsén, M. Davidson, S. Nordholm, O. Orwar and R. N. Zare, *Chem. Phys.*, 1999, **247**, 133–139.
41 E. Boukobza, A. Sonnenfeld and G. Haran, *J. Phys. Chem. B*, 2001, **105**, 12165–12170.
42 B. Okumus, T. J. Wilson, D. M. J. Lilley and T. Ha, *Biophys. J.*, 2004, **87**, 2798–2806.
43 A. K. Boal and A. C. Rosenzweig, *Chem. Rev.*, 2009, **109**, 4760–4779.
44 A. J. Brenner and E. D. Harris, *Anal. Biochem.*, 1995, **226**, 80–84.
45 P. S. Cremer and S. G. Boxer, *J. Phys. Chem. B*, 1999, **103**, 2554–2559.
46 S. K. Sarkar, N. M. Andoy, J. J. Benitez, P. R. Chen, J. S. Kong, C. He and P. Chen, *J. Am. Chem. Soc.*, 2007, **129**, 12461–12467.
47 T. Ha, *Methods*, 2001, **25**, 78–86.
48 I. Rasnik, S. A. McKinney and T. Ha, *Nat. Methods*, 2006, **3**, 891–893.
49 L. Banci, I. Bertini, V. Calderone, N. Della-Malva, I. C. Felli, S. Neri, A. Pavelkova and A. Rosato, *Biochem. J.*, 2009, **422**, 37–42.
50 A. Rodriguez-Granillo, A. Crespo, D. A. Estrin and P. Wittung-Stafshede, *J. Phys. Chem. B*, 2010, **114**, 3698–3706.

